Microscopic properties of lithium, sodium, and magnesium battery anode materials related to possible dendrite growth

Markus Jäckle, and Axel Groß

Citation: The Journal of Chemical Physics **141**, 174710 (2014);
View online: https://doi.org/10.1063/1.4901055
View Table of Contents: http://aip.scitation.org/toc/jcp/141/17
Published by the American Institute of Physics

Articles you may be interested in

Annealing kinetics of electrodeposited lithium dendrites
The Journal of Chemical Physics **143**, 134701 (2015); 10.1063/1.4930014

Electrolyte decomposition on Li-metal surfaces from first-principles theory
The Journal of Chemical Physics **145**, 204701 (2016); 10.1063/1.4967810

A climbing image nudged elastic band method for finding saddle points and minimum energy paths
The Journal of Chemical Physics **113**, 9901 (2000); 10.1063/1.1329672

Lithium fiber growth on the anode in a nanowire lithium ion battery during charging
Applied Physics Letters **98**, 183107 (2011); 10.1063/1.3585655

A consistent and accurate ab initio parametrization of density functional dispersion correction (DFT-D) for the 94 elements H-Pu
The Journal of Chemical Physics **132**, 154104 (2010); 10.1063/1.3382344

Real-time observation of lithium fibers growth inside a nanoscale lithium-ion battery
Applied Physics Letters **99**, 123113 (2011); 10.1063/1.3643035

Microscopic properties of lithium, sodium, and magnesium battery anode materials related to possible dendrite growth

Markus Jäckle and Axel Groß
Institute of Theoretical Chemistry, Ulm University, 89069 Ulm, Germany and Helmholtz Institut Ulm (HIU) Electrochemical Energy Storage, 89069 Ulm, Germany

(Received 15 September 2014; accepted 23 October 2014; published online 7 November 2014)

Lithium and magnesium exhibit rather different properties as battery anode materials with respect to the phenomenon of dendrite formation which can lead to short-circuits in batteries. Diffusion processes are the key to understanding structure forming processes on surfaces. Therefore, we have determined adsorption energies and barriers for the self-diffusion on Li and Mg using periodic density functional theory calculations and contrasted the results to Na which is also regarded as a promising electrode material in batteries. According to our calculations, magnesium exhibits a tendency towards the growth of smooth surfaces as it exhibits lower diffusion barriers than lithium and sodium, and as an hcp metal it favors higher-coordinated configurations in contrast to the bcc metals Li and Na. These characteristic differences are expected to contribute to the unequal tendencies of these metals with respect to dendrite growth. © *2014 AIP Publishing LLC*. [http://dx.doi.org/10.1063/1.4901055]

I. INTRODUCTION

Electrochemical energy storage systems are a crucial component of modern technologies for renewable energy, electrified transportation, and smart grids. In spite of significant progress in recent years there are still severe challenges in battery operation with respect to gravimetric and volumetric energy densities, recyclability and life time, recharging speed, and safety issues.[1–5] Because of these problems, it is unfortunate that our knowledge of the structures and processes occurring in batteries on a microscopic level is still incomplete.[4,6] Among other, lithium air batteries are promising candidates for a battery technology with high gravimetric and volumetric energy density. Yet, it is fair to say that there are still severe problems associated with their usage.[7,8] One of the problems associated with the use of lithium as an anode material is the possible formation of Li dendrites.[8–11]

Their presence can cause short-circuits which lead to irreversible battery damage and hazards such as battery fires. With pure lithium anodic batteries this safety issue becomes even more important, not only because of safety itself, but also because of issues like cyclability, loss of anode material, and pollution of the electrolyte by dendritic deposits.[8–11] This prevents replacing the graphite anodes in lithium-ion batteries by lithium metal anodes although lithium anodes have a significantly higher energy density. Current theories of the dendrite formation suggest that through imperfections in the solid electrolyte interphase (SEI), local deviations in the surface charge occur which then tend to attract more lithium deposition than an ideal surface.[7,12,13] Furthermore, lithium/polymer interfaces were treated using linear elasticity theory.[14] This study demonstrated the importance of electrolyte mechanical properties with respect to the amplification of surface roughness. The influence of the electrolyte was also addressed in a recent experimental study[15] which, motivated by joint density functional theory calculations,[16] showed that electrolytes containing lithium halide salts as additives suppress the tendency towards dendride formation. On the other hand, another recent work claims that subsurface structures in lithium electrodes play a crucial role in dendrite formation.[17]

One candidate for substituting lithium in batteries would be magnesium.[18–20] Although the gravimetric energy density of Mg is only half of the one of Li, its volumetric energy density is even higher as Mg can carry two elementary charge units. Furthermore, Mg is much more abundant in the earth crust making it also economically very attractive.

In addition, recent *in situ* studies of the Mg deposition-dissolution performance suggest that Mg does not tend to form agglomerates upon deposition, but instead shows a trend to form uniform structures.[21,22] This indicates that magnesium most likely does not form dendrites. Furthermore, alloying Mg with Li also suppresses the tendency towards dendrite growth.[23]

Because of the devastating impact of dendrite growth on battery performance it is important to understand its origin. Certainly, the process of dendrite formation in an operating battery is rather intricate due to the complex structure of the electrode/electrolyte interface involving the solid-electrolyte interphase. For a complete understanding of the dendrite growth under battery operation the consideration of the complex environment within the SEI is mandatory taking the correct electrochemical conditions properly into account.[24] However, it is currently not possible to model dendrite growth atomistically in a realistic electrochemical environment. Coarse-grained models have been used to identify the factors influencing Li dendrite growth.[25] The simulations, for example, indicate that the dendrite formation propensity increases with electrode overpotential.

However, all the models and mechanisms discussed so far do not include element-specific details. Hence they are not able to discriminate between different metals. Thus they cannot explain why Li exhibits dendrite growth and Mg not.

 © 2014 AIP Publishing LLC

Since a full realistic atomistic modeling of dendrite growth is currently not possible, as a first step a reductionistic approach is necessary in which basic metallic properties related to dendrite growth are compared.

Such an approach was employed in a recent density functional theory (DFT) study[26] which concluded that the stronger bonding between Mg atoms compared to Li might be decisive as the diffusion barriers of both materials are rather similar. These findings were derived by considering several low-dimensional metallic structures.[26] However, the relevance of the different structures in a growth process was not assessed. By concentrating on the energetically most favorable metal structures which are most abundant we derive at different conclusions than the previous study.[26]

Note that specific metal structures growing on electrodes are controlled by diffusion processes.[27–31] Hence a crucial part in the modeling of dendrite growth is the determination of metal self-diffusion paths and the corresponding diffusion barriers.[32] We have used DFT calculations to study surface energies, adsorpion energies in homoepitaxy, and self-diffusion barriers of Li and Mg. We contrast the results with another promising alkali metal for battery applications, sodium.[33] To the best of our knowledge, such a comparison of the basic properties of these three battery anode materials based on first-principles calculations has not been made before.

Our results indicate that magnesium exhibits a tendency towards the growth of smooth surfaces as it exhibits low diffusion barriers and favors high-coordinated configurations. These properties might contribute to the observed lack of dendrite growth in magnesium batteries. In contrast, lithium and sodium self-diffusion on the energetically most favorable surface terminations is hindered by higher barriers, and Li and Na as bcc metals exhibit a lower tendency towards high-coordinated configurations. This could explain the higher propensity of Li towards dendrite growth.

II. CALCULATIONAL METHODS

Periodic DFT calculations have been performed using the Vienna *Ab Initio* Simulation Package (VASP)[34,35] within the generalized gradient approximation (GGA) to account for exchange correlation effects employing the functional of Perdew, Burke, and Ernzerhof[36] which is well-suited to describe metallic properties.[37,38] The core electrons are represented by projector augmented wave (PAW) pseudopotentials[39] as supplied in VASP[40] with a cutoff energy of 400 eV. As shown below, this cutoff is sufficient to reproduce properties of the considered metals such as bulk cohesive energy and lattice constants.

The Brillouin zone integration for bulk calculations has been performed on a $9 \times 9 \times 9$ k-point grid. The electrode surfaces are modeled by 5-layer slabs. The comparison of calculated surface energies for 5-layers slabs with those derived from calculations for 7- and 9-layer slabs indicates that 5-layer slabs are thick enough to reliably model the electrode surfaces. Adsorption energies and diffusion paths have been determined within a 4×4 geometry using a $5 \times 5 \times 1$ k-point grid. The relaxation in the calculations has been performed until the forces were smaller than 0.001 eV/Å and the total free energy change was smaller than 0.0001 eV. For all adsorption calculations, the atoms of the uppermost two surface layers were allowed to relax in all directions.

III. RESULTS

A. Bulk properties

First note that the two alkali metals lithium and sodium crystallize in the bulk-centered cubic (bcc) structure with an eightfold coordination whereas the alkaline earth metal magnesium assumes a hexagonal close-packed (hcp) structure with a twelvefold coordination.[41]

For lithium, a lattice constant of $a = 3.44$ Å has been calculated, which only slightly deviates from the experimentally retrieved value of $a = 3.49$ Å[41] and is in good agreement with other calculated values.[42] The calculated lattice constant of sodium is $a = 4.19$ Å, again in good agreement with the experimental value of $a = 4.29$ Å. For magnesium, the hcp lattice constants were calculated to be $a = 3.19$ Å and $c = 5.18$ Å which again corresponds to a small deviation from the literature values of $a = 3.21$ Å and $c = 5.21$ Å,[41,43,44] but are in accordance with extrapolated 0 K values[43,44] and also with other calculated values of $a = 3.18$ Å and $c = 5.14$ Å.[45]

The cohesive energies have been calculated by subtracting the calculated energy of an isolated metal-atom from the energy of this atom within the bulk:

$$E_{coh} = -(E_{bulk} - E_{atom}). \quad (1)$$

The calculated values are compared with experimental ones in Table I. The cohesive energy for lithium was evaluated to be 1.61 eV/atom, the experimental value is 1.63 eV/atom,[41] another calculated value is 1.61 eV/atom.[42] In the case of sodium, the calculated value of 1.10 eV/atom is close to the experimental value of 1.11 eV/atom.[41] For hcp magnesium the cohesive energy was calculated to be 1.50 eV/atom while the experimental value is 1.51 eV/atom,[41] both close to a previously calculated value of 1.50 eV/atom.[45]

Note that the cohesive energies of Mg and Li are rather similar, and regarding Li as being eightfold coordinated and Mg as being twelvefold coordinated, the energy per bulk metal-metal bond is considerably larger in Li than in Mg. Thus the comparison of the bulk properties does not support the conclusion of the previous computational study[26] that the Mg–Mg bond is stronger than the Li–Li bond.

B. Surface energies

Surface properties are not only important because they determine the equilibrium shape, but also help understanding

TABLE I. Cohesive energies in eV/atom.

Cohesive energies (eV/atom)	Li	Na	Mg
Expt.[41]	1.63	1.11	1.51
This work	1.61	1.10	1.50

TABLE II. Calculated surface energies of Li, Na, and Mg surfaces compared to previous studies.[42,45,46]

	Li(001)	Li(011)	Li(111)	Na(001)	Na(011)	Na(111)	Mg(0001)
E_{surf} (eV/atom) this work	0.34	0.26	0.54	0.24	0.17	0.50	0.28
γ (J/m^2) this work	0.46	0.49	0.53	0.22	0.22	0.26	0.52
γ (J/m^2) other works	0.47[42]	0.50[42]	0.56[42]	0.23[46]	0.22[46]	0.28[46]	0.55[45]

crystal growth phenomena.[47,48] Here, we determine the most stable surfaces of the bcc metals lithium and sodium among the low-index (001), (011), and (111) surfaces. For the hcp metal magnesium, the close-packed (0001) surface is the most stable one.[45]

The surface energies have been estimated by calculating the energy of a 5-layer slab with the first two layers on each side being relaxed and subtracting the energy of the atoms in the bulk according to

$$E_{\text{surf}} = \frac{1}{2N}(E_{slab} - N \cdot E_{coh})). \quad (2)$$

E_{surf} represents the calculated surface energy per atom in eV/Å. Furthermore, we have converted these values into surface energies per area γ in J/m^2. The resulting numbers are collected in Table II. The table also demonstrates that our calculated values compare well with previously calculated numbers.[42,45,46] With respect to the lithium surfaces we note that the most stable one is the square (001) surface, followed in stability by the (011) and (111) surface. This order is typical for bcc surfaces as the hexagonal bcc(111) surface is rather open with a relatively large distance between the surface atoms. For sodium, the (001) and (011) surfaces are basically energetically degenerate, Na(111) is slightly less favorable. The surface energies of sodium per area are only one half of those for lithium. This can be understood by the combination of the two facts that first the surface energies per atom of sodium are reduced compared to lithium due to the smaller cohesive energy and that second the lattice constant of sodium is larger than the one of lithium.

For Mg(0001), the calculated surface energy value of 0.52 J/m^2 or 0.28 eV/atom is in good agreement with the literature value of 0.55 J/m^2 or 0.30 eV/atom.[45] Note that the surface energy per area of the hexagonal Mg(0001) surface is rather similar to the one of the square Li(001) surface. As seen in Sec. III A, also the cohesive energies of Li and Mg are rather similar. Regarding these energetics, there is no dramatic difference between Li and Mg so that these properties do not give a first hint as to why there is such a difference between the two metals with respect to dendrite growth.

TABLE III. Adsorption energies of Li, Na, and Mg adatoms in homoepitaxy on different adsorption sites.

E_{ads} (eV)	bridge (b)	hollow (h)		top (t)
Li(001)	− 1.13	−1.28		− 1.05
Na(001)	− 0.75	−0.91		− 0.62
	bridge (b)	fcc	hcp	top (t)
Mg(0001)	− 0.57	− 0.59	− 0.57	− 0.44

C. Adsorption energies

As this paper aims at contributing to the long-term goal of clarifying why lithium grows dendrites and magnesium does not, it is of central interest how strong the bonding of surface adatoms is which might impose irregularities that could contribute to dendritic growth. The adsorption properties were calculated for the most stable surfaces which are the (001)-surface of lithium and sodium and the (0001)-surface of magnesium.

The adsorption energies E_{ads} have been calculated by subtracting the energy of the clean metal electrode E_{slab} and the energy of a single adsorbate atom E_{atom} from the energy of the system with the relaxed adsorbate E_{sys}:

$$E_{\text{ads}} = E_{\text{sys}} - E_{\text{slab}} - \text{E}_{\text{atom}}. \quad (3)$$

The adsorption energies of Li, Na, and Mg adatoms on the high-symmetry sites of their respective most stable surface terminations are collected in Table III. As far as the bcc surfaces of Li and Na are concerned, the fourfold hollow site is clearly favored compared to the bridge and top sites. In contrast, on Mg(0001), the threefold hollow sites and the bridge site are energetically almost degenerate. The most favorable adsorption positions are illustrated in Fig. 1.

Li adsorption energies are larger in magnitude than the Na adsorption energies which can be explained by the larger cohesive energy of Li. Note also that Li adsorption on Li(001) is stronger than Mg adsorption on Mg(0001) which might be caused by the higher coordination in the fourfold hollow site of the bcc(001) surface compared to the threefold hollow fcc site on hcp(0001).

A further important property concerning the growth of metal structures is the interaction energy between adatoms since this governs how favorable it is for adatoms to form islands.[29,49] Therefore, we have calculated the interaction energy E_{int} between two adatoms within the chosen supercells which is the difference between the adsorption energy of two

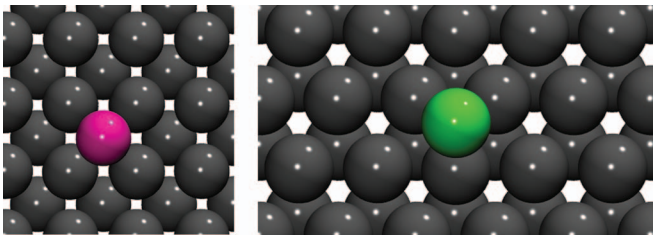

FIG. 1. Most favorable adsorption positions in homoepitaxy on Li(001) and Mg(0001).

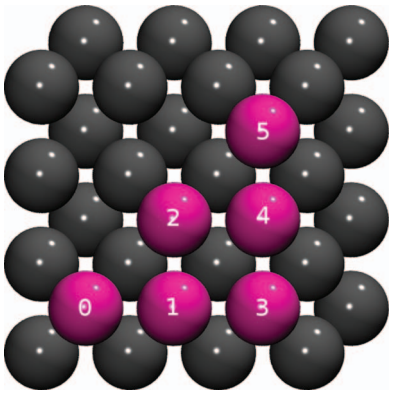

FIG. 2. Possible positions of two adatoms within the (4 × 4)bcc(001) surface unit cell.

adatoms in the surface unit cell and the adsorption energies of two isolated adatoms.

The possible configurations for two adatoms within the (4 × 4)bcc(001) surface unit cell are illustrated in Fig. 2. Site 0 corresponds to the position of the first adatom, sites 1-5 illustrate the possible, geometrically inequivalent position of the second adatom. In the determination of E_{int}, the adatoms together with the two uppermost substrate layers were fully allowed to relax.

The calculated dimer interaction energies for Li(001) are collected in Table IV. For the two shortest separations with the second adatom in site 1 or 2 there is a small attractive interaction, whereas for the second adatom in sites 3, 4, and 5 there is almost no interaction. So in general there is only a weak interaction between Li adatoms in the fourfold hollow sites of Li(001) which is also reflected by the fact that there is only very little relaxation of the dimer atoms compared to their isolated configuration. This small interaction energy is possibly a consequence of the large adsorption energy of single adatoms which reduces the attraction to other adatoms in a bond-order conservation picture. Furthermore, it should be noted that the two adatoms at adjacent adsorption sites do not correspond to nearest neighbors which might also contribute to the relatively weak interaction. The other considered alkali metal, sodium, exhibits very similar properties compared to lithium with respect to the interaction between two adatoms.

For the case of Mg dimers within the (4 × 4)hcp(0001) surface unit cell, we considered the three inequivalent configurations illustrated in Fig. 3(a). As Table IV demonstrates, there is now a relatively large interaction energy for the two Mg adatoms in adjacent fcc hollow sites which is three times larger than for the corresponding Li dimer. Using bond-order conservation arguments, this stronger interaction might be caused by the lower adsorption energy of Mg on Mg(0001). Note also that on the hcp(0001) surfaces two adatoms at adjacent adsorption sites are nearest neighbors. The attractive interaction even results in a further reduced distance between the two Mg adatoms which is lower by −0.28 Å compared to the bulk nearest neighbor distance, as illustrated in Fig. 3(b).

TABLE IV. Interaction energies in eV and separations for two Li, Na, and Mg adatoms in homoepitaxy with the sites labeled according to Figs. 2 and 3.

2nd adatom site	1	2	3	4	5
Li E_{int} (eV)	− 0.17	− 0.05	0.02	0.02	0.03
Li seperation (Å)	3.20	3.91	6.89	7.70	9.74
Na E_{int} (eV)	− 0.14	− 0.03	− 0.02	− 0.02	0.00
Na seperation (Å)	3.72	5.87	8.38	9.37	11.85
Mg E_{int} (eV)	− 0.50	0.00	− 0.50		
Mg seperation (Å)	2.94	6.41	2.95		

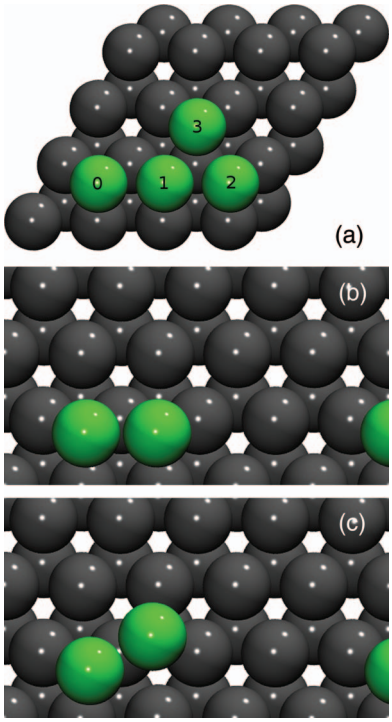

FIG. 3. (a) Possible positions of two adatoms within the (4 × 4)hcp(0001) surface unit cell. (b, c) Fully relaxed geometries for the second Mg adatom initially in site 1 and 3, respectively.

For the Mg dimer at site 0 and 2, there is basically no interaction any more, however, for the Mg adatoms initially at sites 0 and 3, there is again a strong interaction. This is caused by the fact that upon relaxation the second adatom does not stay at site 3 but is attracted towards the hcp hollow site adjacent to site 0, as illustrated in Fig. 3(c). The very similar interaction energies for the dimers 0-1 and 0-3 are a consequence of the basically identical distances within these two dimer pairs, but note that the second atom in the two resulting configurations sits in a fcc and hcp site, respectively.

Concluding this section, there is a stronger interaction between Mg adatoms on Mg(0001) than between Li and Na adatoms on Li(001) and Na(001), respectively, which is most likely a consequence of the lower adsorption energy of Mg adatoms and the closer distance of the adatoms at adjacent adsorption sites. This indicates that Mg exhibits a more pronounced tendency to form adatom agglomerates, as predicted by the nucleation theory of growth,[29,49] whereas Li

TABLE V. Activation barriers for hopping self-diffusion on Li(001), Li(111), Na(001), and Mg(0001). For Li(001), in addition the barrier in the exchange mechanism is given.

	E_{diff} (eV)	Mechanism
Li(001)	0.14	Hopping
Li(001)	0.21	Exchange
Li(111)	0.41	Hopping
Na(001)	0.16	Hopping
Mg(0001)	0.02	Hopping

and Na adatoms have a more pronounced tendency to stay isolated.

D. Diffusion properties

Diffusion barriers play an important role in the homoepitaxial growth mechanism.[27–31] In a general sense it can be said that the faster the diffusion is, the smoother the resulting surface structures are because the surface atoms can join to form complete surface layers, or vice versa, the slower the diffusion is, the rougher the resulting surface structures are since complete surface layers are not likely to be formed.

Typically, in diffusion processes one considers the so-called hopping mechanism with an atom propagating from the most favorable adsorption position to the next one via the neighboring bridge site. Thus the activation energy for hopping diffusion E_{diff} can be determined by the difference between the most favorable adsorption energy and the adsorption energy at the bridge position which have already been listed in Table III. In addition, in order to get an better idea about the energetics involved in the hopping diffusion, we have determined the whole potential energy surface of a Li adatom on Li(001) and of a Mg adatom on Mg(0001) that are plotted in Fig. 4. The resulting diffusion barriers are listed in Table V.

On Li(001) and Na(001), hopping diffusion is hindered by barriers of 0.14 eV and 0.16 eV, respectively, i.e., they are rather similar. In contrast, on Mg(0001) hopping diffusion is only hindered by the rather low barrier of 0.02 eV. As Table III and Fig. 4 indicate, this barrier is due to the propagation from the fcc to the hcp hollow site which is slightly less favorable whereas diffusion from the hcp hollow to the fcc hollow site is hardly hindered by any barrier.

We have also considered Li self-diffusion on the hexagonal Li(111) surface which is, however, hindered by a rather high barrier of 0.41 eV. This high barrier is due to the open nature of the bcc(111) surface which leads to a large energetic difference between the threefold hollow and the bridge positions.

The hopping mechanism is mainly operative on close-packed metal surfaces. On square (100) surfaces such as Pt(100)[50] or Ir(100),[51] in fact another diffusion mechanism has been observed, namely the so-called exchange mechanism in which the adatom displaces a surface atom which then becomes the adatom.

Whereas in the hopping mechanism at the transition state the hopping atom is in a twofold coordination, in the exchange mechanism on (100) surfaces there are two atoms in a threefold coordination at the transition state. The fact whether one atom in a twofold coordination is more favorable than two atoms in a threefold coordination then determines which mechanism is operative. The exchange mechanism is preferred at metal surfaces that favor a threefold coordination with the three-valent aluminum being the prototypical example.[52,53] In addition, the exchange mechanism can also be more favorable for diffusion across the steps of a stepped surface[31] since the hopping mechanism across a step is hindered by the relatively large Ehrlich-Schwoebel barrier[54,55] caused by the low coordination at the transition state for diffusion across the step.[47]

However, as the exchange mechanism involves the cooperative motion of several surface atoms, it is not trivial to determine the activation barrier. In order to find the minimum energy path (MEP) in the exchange mechanism of Li self-diffusion on Li(001) we have used the nudged elastic band method (NEB)[56] that corresponds to an automatic search routine for finding the MEP between specified initial and final states and that is well-suited to yield the reaction path of complex processes on surfaces.[57]

Figure 5 shows snapshots of the atomic configuration along the minimum energy path for the self-diffusion of Li on Li(001) in the exchange mechanism which is hindered by a barrier of 0.21 eV that is slightly larger than the barrier for the hopping mechanism (see Table V).

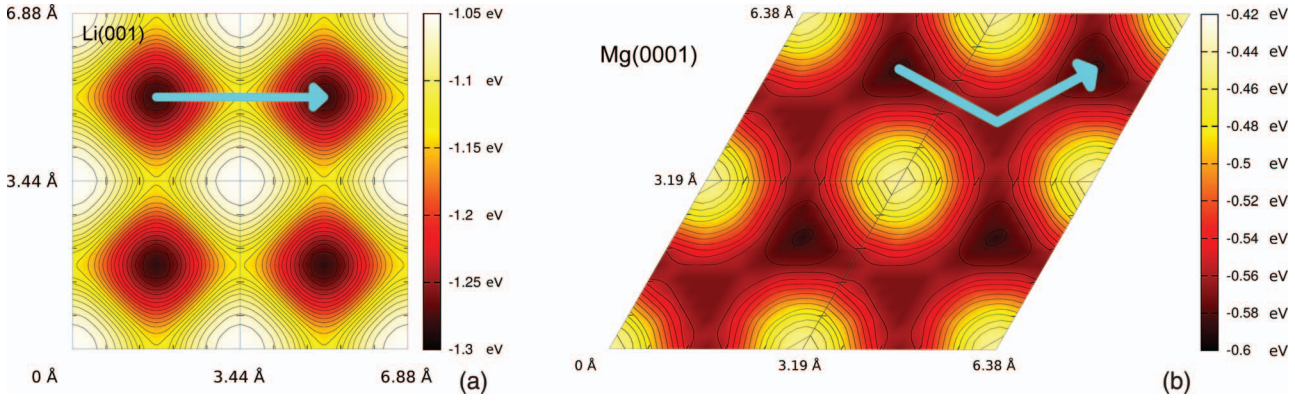

FIG. 4. Potential energy surfaces of (a) a Li adatom on Li(001) and (b) a Mg adatom on Mg(0001). The contour spacing in (a) is 0.05 eV while it is 0.02 eV in (b).

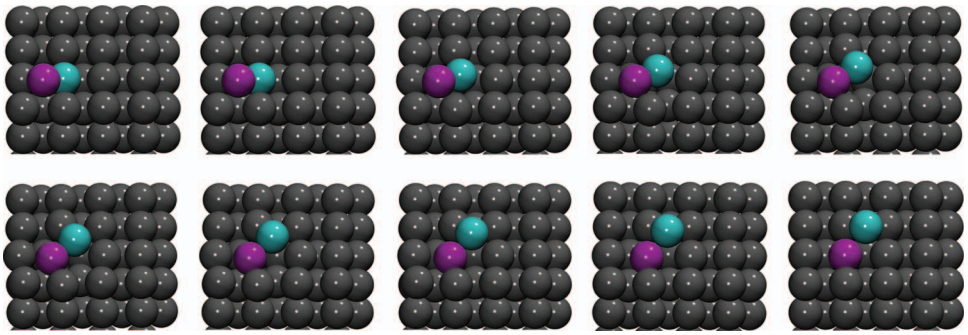

FIG. 5. Snapshots of the atomic configuration along the minimum energy path for the self-diffusion of Li on Li(001) in the exchange mechanism.

However, in a Arrhenius picture the rate with which a certain process occurs does not only depend on the activation barrier via the Boltzmann factor, but also on the prefactor. We have used the simplified transition state theory (STST)[58] in order to estimate the rates for hopping and exchange diffusion,

$$k = n_p \nu_0 exp\left(-\frac{E_{diff}}{k_B T}\right). \quad (4)$$

In this approximation, the prefactor is simply given by the attempt frequency ν_0[59] along the one-dimensional minimum energy path multiplied by the factor n_p which takes the number of geometrically equivalent processes into account. For both the exchange as well as the hopping mechanism on Li(001), $n_p = 4$ due to the fourfold symmetry of both diffusion mechanisms.

The attempt frequencies that are listed in Table VI have been derived from an harmonic fit to the potential curves for the exchange and the hopping mechanism. For the harmonic frequency of the exchange mechanism, the effective mass of two lithium atoms was used. It turns out that the attempt frequency is by about 40% larger for the exchange than for the hopping mechanism so that eventually the rate of the exchange mechanism at room temperature is 11 times smaller than for the hopping mechanism. This means that diffusion on Li(001) is dominated by hopping but exchange processes also contribute to diffusion. These rates might then enter a kinetic Monte Carlo (KMC) algorithm[60] which is the state-of-the-art method to simulate growth processes on surfaces on a macroscopic time scale and a mesoscopic length scale.[28,29,59]

Even with taking into account the exchange mechanism it is still clear that self-diffusion on Li(001) and Na(001) is much slower than on Mg(0001) with its close-packed hexagonal structure. This means that diffusion favors a smooth surface growth on Mg(0001) to a much larger extent than on Li(001) and Na(001).

TABLE VI. Attempt frequencies ν_0 and rates k at room temperature for the exchange and hopping self-diffusion on Li(001).

	Exchange	Hopping
ν_0 (s^{-1})	2.13×10^{13}	1.53×10^{13}
k (s^{-1})	2.16×10^{10}	2.45×10^{11}

IV. SUMMARY AND CONCLUSION

Motivated by the observed differences with respect to dendrite growth, the basic properties of Li and Mg electrodes with respect to growth processes have been studied by periodic density functional theory calculations and contrasted to the properties of Na. Whereas Li and Na crystallize in the body-centered cubic structure, Mg has a hexagonal close-packed structure. The cohesive energies of Li and Mg are rather similar, Na has a smaller cohesive energy. The square (001) terminations correspond to the energetically favorable surface structures of Li and Na in contrast to the smooth hexagonal Mg(0001) surface.

Because of the more open structure of the bcc(001) surface, adsorption in homoepitaxy on Li(001) and Na(001) is stronger than on Mg(0001). On the other hand, the interaction of two adjacent adatoms is stronger on Mg(0001) than on Li(001) and Na(001) which can be understood on the basis of bond-order arguments. Furthermore, self-diffusion on Mg(0001) is much more facile than on Li(001) and Na(001), even if additionally exchange processes on the bcc(001) surfaces are taken into account.

All these properties indicate that metal growth on Mg(0001) should lead to much smoother structures than on Li(001) and Na(001). Self-diffusion on Mg(0001) is rather fast, and in addition the interaction energy between Mg adatoms is large so that stable nucleation centers for thin-film growth can readily form. This tendency for the growth of smooth structures might already be an important reason why Mg electrodes do not exhibit dendrite growth. Li, on the other hand, shows a stronger tendency towards the growth of a rough surface which supports the formation of dendrites. Furthermore, based on the calculations, Na should show similar growth properties as Li. It should be mentioned that the differences between Li and Mg with respect to their growth properties can qualitatively be derived from the fact that Mg as a hcp metal with a twelvefold coordination in the bulk favors compact high-coordinates structures to a larger extent than Li as a bcc metal with eightfold coordination in the bulk.

In this study, the complex environment of metal anodes in batteries has not been considered at all. However, existing models of dendrite growth in batteries are typically not element-specific, and consequently they do not allow to discriminate between Li and Mg. Therefore we are convinced that the characteristic differences between Li and Mg with respect to elementary properties relevant for growth identified in

this study significantly contribute to the observed differences in dendrite formation in batteries with Li and Mg anodes.

ACKNOWLEDGMENTS

Useful discussions with Tanglaw Roman, Sung Sakong, Nicolas Hörmann, Fernanda Juarez, and Florian Gossenberger are gratefully acknowledged. The calculations have been made possible through generous supply of computer time at the Leibniz Rechenzentrum (LRZ) in Munich and at a computer cluster financed through the stimulus programme "Electrochemistry for Electromobility" of the German Ministry of Education and Science (BMBF).

[1] J. Goodenough, J. Solid State Electrochem. **16**, 2019 (2012).
[2] B. Kang and G. Ceder, Nature **458**, 190 (2009).
[3] K. Zaghib, J. B. Goodenough, A. Mauger, and C. Julien, J. Power Sources **194**, 1021 (2009).
[4] G. Ceder and B. Kang, J. Power Sources **194**, 1024 (2009).
[5] J. H. Pikul, H. G. Zhang, J. Cho, P. V. Braun, and W. P. King, Nat. Commun. **4**, 1732 (2012).
[6] N. Hörmann and A. Groß, J. Solid State Electrochem. **18**, 1401 (2014).
[7] J. Christensen, P. Albertus, R. S. Sanchez-Carrera, T. Lohmann, B. Kozinsky, R. Liedtke, J. Ahmed, and A. Kojic, J. Electrochem. Soc. **159**, R1 (2012).
[8] K. Xu, Chem. Rev. **104**, 4303 (2004).
[9] W.-S. Kim and W.-Y. Yoon, Electrochim. Acta **50**, 541 (2004).
[10] K. Nishikawa, T. Mori, T. Nishida, Y. Fukunaka, M. Rosso, and T. Homma, J. Electrochem. Soc. **157**, A1212 (2010).
[11] G. Girishkumar, B. McCloskey, A. C. Luntz, S. Swanson, and W. Wilcke, J. Phys. Chem. Lett. **1**, 2193 (2010).
[12] A. Schechter and D. Aurbach, Langmuir **15**, 3334 (1999).
[13] Y. S. Cohen, Y. Cohen, and D. Aurbach, J. Phys. Chem. B **104**, 12282 (2000).
[14] C. Monroe and J. Newman, J. Electrochem. Soc. **152**, A396 (2005).
[15] Y. Lu, Z. Tu, and L. A. Archer, Nat. Mater. **13**, 961 (2014).
[16] D. Gunceler, K. Letchworth-Weaver, R. Sundararaman, K. A. Schwarz, and T. A. Arias, Modell. Simul. Mater. Sci. Eng. **21**, 074005 (2013).
[17] K. J. Harry, D. T. Hallinan, D. Y. Parkinson, A. A. MacDowell, and N. P. Balsara, Nat. Mater. **13**, 69 (2014).
[18] P. Novak, R. Imhof, and O. Haas, Electrochim. Acta **45**, 351 (1999).
[19] H. D. Yoo, I. Shterenberg, Y. Gofer, G. Gershinsky, N. Pour, and D. Aurbach, Energy Environ. Sci. **6**, 2265 (2013).
[20] R. Mohtadi and F. Mizuno, Beilstein J. Nanotechnol. **5**, 1291 (2014).
[21] Q. S. Zhao and J. L. Wang, Electrochim. Acta **56**, 6530 (2011).
[22] D. Aurbach, Y. Cohen, and M. Moshkovich, Electrochem. Solid-State Lett. **4**, A113 (2001).
[23] T. J. Richardson and G. Chen, J. Power Sources **174**, 810 (2007).
[24] S. Schnur and A. Groß, Catal. Today **165**, 129 (2011).
[25] M. Z. Mayers, J. W. Kaminski, and T. F. Miller, J. Phys. Chem. C **116**, 26214 (2012).
[26] C. Ling, D. Banerjee, and M. Matsui, Electrochim. Acta **76**, 270 (2012).
[27] T. Michely, M. Hohage, M. Bott, and G. Comsa, Phys. Rev. Lett. **70**, 3943 (1993).
[28] P. Ruggerone, A. Kley, and M. Scheffler, Prog. Surf. Sci. **54**, 331 (1997).
[29] H. Brune, Surf. Sci. Rep. **31**, 125 (1998).
[30] M. E. Quayum, S. Ye, and K. Uosaki, J. Electroanal. Chem. **520**, 126 (2002).
[31] X. Lin, A. Dasgupta, F. Xie, T. Schimmel, F. Evers, and A. Groß, Electrochim. Acta **140**, 505 (2014).
[32] H. Jónsson, Annu. Rev. Phys. Chem. **51**, 623 (2000).
[33] B. Dunn, H. Kamath, and J.-M. Tarascon, Science **334**, 928 (2011).
[34] G. Kresse and J. Furthmüller, Phys. Rev. B **54**, 11169 (1996).
[35] G. Kresse and J. Furthmüller, Comput. Mater. Sci. **6**, 15 (1996).
[36] J. P. Perdew, K. Burke, and M. Ernzerhof, Phys. Rev. Lett. **77**, 3865 (1996).
[37] A. Groß, J. Comput. Theor. Nanosci. **5**, 894 (2008).
[38] A. Groß, J. Phys.: Condens. Matter **21**, 084205 (2009).
[39] P. E. Blöchl, Phys. Rev. B **50**, 17953 (1994).
[40] G. Kresse and D. Joubert, Phys. Rev. B **59**, 1758 (1999).
[41] C. Kittel, *Introduction to Solid State Physics*, 8th ed. (John Wiley & Sons, New York, 2004).
[42] K. Doll, N. M. Harrison, and V. R. Saunders, J. Phys.: Condens. Matter **11**, 5007 (1999).
[43] I. Baraille, C. Pouchan, M. Causà, and F. Marinelli, J. Phys.: Condens. Matter **10**, 10969 (1998).
[44] W. Köster and H. Franz, Int. Mater. Rev. **6**, 1 (1961).
[45] E. Wachowicz and A. Kiejna, J. Phys.: Condens. Matter **13**, 10767 (2001).
[46] C. Fiolhais and L. M. Almeida, Int. J. Quantum Chem. **101**, 645 (2005).
[47] A. Groß, *Theoretical Surface Science – A Microscopic Perspective*, 2nd ed. (Springer, Berlin, 2009).
[48] L. Vitos, A. V. Ruban, H. L. Skriver, and J. Kollár, Surf. Sci. **411**, 186 (1998).
[49] J. A. Venables, Phys. Rev. B **36**, 4153 (1987).
[50] G. L. Kellogg and P. J. Feibelman, Phys. Rev. Lett. **64**, 3143 (1990).
[51] C. Chen and T. T. Tsong, Phys. Rev. Lett. **64**, 3147 (1990).
[52] P. J. Feibelman, Phys. Rev. Lett. **65**, 729 (1990).
[53] R. Stumpf and M. Scheffler, Phys. Rev. B **53**, 4958 (1996).
[54] G. Ehrlich and F. G. Hudda, J. Chem. Phys. **44**, 1039 (1966).
[55] R. L. Schwoebel and E. J. Shipsey, J. Appl. Phys. **37**, 3682 (1966).
[56] G. Henkelman and H. Jónsson, J. Chem. Phys. **113**, 9978 (2000).
[57] S. Sakong, C. Mosch, A. Lozano, H. F. Busnengo, and A. Groß, ChemPhysChem **13**, 3467 (2012).
[58] A. F. Voter, Phys. Rev. B **34**, 6819 (1986).
[59] C. Sendner and A. Groß, J. Chem. Phys. **127**, 014704 (2007).
[60] K. A. Fichthorn and W. H. Weinberg, J. Chem. Phys. **95**, 1090 (1991).